

Claudio L. A. Berli^{1,2}

¹INTEC (Universidad Nacional del Litoral-CONICET), Santa Fe, Argentina

²Facultad de Ingeniería y Ciencias Hídricas, UNL, Santa Fe, Argentina

Received August 31, 2012

Revised December 5, 2012

Accepted December 6, 2012

Review

The apparent hydrodynamic slip of polymer solutions and its implications in electrokinetics

The apparent hydrodynamic slip of polymer solutions is a result of polymer depletion at channel walls, and its fluid dynamic effects are well known. This work reviews the evidences of apparent slip in electrokinetics, and discusses practical consequences in the following fields: (i) electrokinetic transport of polymer solutions in microchannels, which is of interest for the design and operation of microfluidic chips, particularly for electrophoresis; (ii) electroosmotic pumping, where it has been observed that the employment of polymer solutions greatly enhances the output pressure; and (iii) electrokinetic energy conversion, where the apparent slip also contributes to improve the conversion efficiency. In all cases, critical discussions are taken from basic physical concepts.

Keywords:

Apparent slip / Energy conversion / EOF of polymers / Microfluidics / Wall depletion
DOI 10.1002/elps.201200476

1 Introduction

The necessity to manipulate biofluids and other polymeric liquids in microfluidic chips leads to a renewed interest on the dynamics of complex fluids in small confinements. In addition, the facilities of the new microfluidic technology enable the observation of phenomena that take place at the microscopic level, leading to new discoveries [1]. In fact, the behaviors exhibited by polymeric fluids in microchannels are not only due to its non-Newtonian nature, but also to particular physical effects of the micro/nano scale, notably wall depletion, which has serious implications in electrokinetics.

The existence of polymer-depleted layers in stagnant solutions in contact with solid boundaries is well documented [2–5]. This behavior is observed in nonadsorbing polymers, the concentration of which decreases steeply near the wall. The thickness δ of the depletion layer is in the order of the radius of gyration of macromolecules [5,6]. In addition, when polymer solutions are subjected to flow, the shear-induced migration of macromolecules increases the thickness δ up to values ten times larger than the molecular size [7–9]. The effect leads to the apparent hydrodynamic slip of the bulk polymer solution over the interfacial layer of solvent [10–14]. The same phenomenon has been reported in studies of particle motion in macromolecular media [15].

Here it is important to differentiate the “apparent” slip from the “true” slip that eventually takes place at solid–liquid interfaces. This subject is now at the center of discussions in fluid mechanics, since the classic assumption of no-slip appears to be constantly violated in microfluidic experiments [12, 16, 17]. The phenomenon is rather subtle, involving the hydrophobic/hydrophilic nature of the surface, the presence of gas bubbles, surface roughness, etc. [12, 16–21], and has enormous consequences on electrokinetics as well [22–26]. Nevertheless, the present review restricts itself to the case of apparent slip exhibited by polymer solutions, the solvent of which in principle satisfies the no-slip condition at the solid–liquid interface.

In electrokinetics, the effect of polymer depletion had been first observed in experiments of electrophoresis of particles with polymer solutions as the background fluid [27]. More recently, the phenomenon was reported in experiments of EOF carried out in fused-silica capillaries with solutions of poly-ethylene glycol [28] and carboxy-methyl cellulose [29], as well as in glass microchannels with poly-acrylamide solutions [30]. However, few efforts have been made to take this effect into account in theoretical descriptions [31–33]; the vast majority of articles dealing with calculations of the electrokinetic flow of non-Newtonian fluids (for example [34–38], to mention a few) disregards the fact that fluid properties are nonuniform in the interfacial region, a feature that is inherent to complex fluids. The topic is revisited in this article, with emphasis on the positive consequences for the dynamics of electrokinetic flow, electroosmotic pumping (EOP), and electrokinetic energy conversion.

Correspondence: Dr. Claudio L. A. Berli, INTEC (Universidad Nacional del Litoral-CONICET), Güemes 3450, 3000, Santa Fe, Argentina

E-mail: cberli@santafe-conicet.gov.ar

Fax: +54-342-4550944

Abbreviations: EDL, electrical double layer; EOP, electroosmotic pumping

Colour Online: See the article online to view Figs. 1–4 and 6 in colour.

More precisely, the present work focuses on the implications of apparent slip in the EOF of polymer solutions, and briefly in electrophoresis of colloidal hard spheres through polymer solutions, which is the reciprocal phenomena (considering that electrokinetic effects involve the tangential displacement of a charged solid surface in relation to the fluid in equilibrium with it [39]). The problem of DNA electrophoresis by using entangled polymer matrices [40–42] is not included in this investigation. Another novel and attractive application of polymers in the field of electrophoresis uses hydrogel-filled microchannels [43–45], where special particles can be trapped or immobilized to act as diagnostic tools and biosensors. The dynamics of these polymer networks under the action of time-dependent electric fields is also out of the scope of the present review. Instead, in order to analyze the influence of polymer depletion independently of non-Newtonian phenomena, discussions here are limited to the case of dilute polymer solutions with viscosity $\eta_p = \eta_s(1 + kc_p + \dots)$, where η_s is the solvent viscosity, c_p is the polymer concentration, and k represents the intrinsic viscosity, which is a measure of the molecular size [46]. In addition, steady-state flows in straight microchannels are considered, so that possible elastic and time-dependent effects are minimized.

The first aspect to be considered is the interaction of polymer molecules with solid surfaces, which leads to nonuniform polymer concentration in the proximity of channel walls, with the consequent variation of the local viscosity in relation to the bulk fluid. Next section summarizes the two main phenomena that take place at interfaces: polymer adsorption and polymer depletion. The rest of the work is devoted to the consequences of wall depletion on the electrokinetic flow of polymer solutions.

2 Fundamentals

2.1 Polymer adsorption and the hydrodynamic layer

Polymer solutions are normally constituted by a simple fluid, the solvent, and a certain concentration of dissolved polymers. If the interaction between polymer chains and the surface is attractive, polymer molecules adhere to the wall [2–5, 47, 48], then the polymer segment concentration increases abruptly near the surface. This behavior is observed for neutral and charged polymers, and the extent of the adsorption depends on the pH of the medium, ionic strength, polymer concentration, and temperature.

The consequences of polymer adsorption on electroosmosis were described several years ago [49]. It is easy to infer that the EOF is strongly diminished due to the fact that the viscosity of the fluid adjacent to the wall increases significantly [49–51]. Another crucial aspect is that adsorbed polymers modify both the sign and magnitude of ζ -potential, depending on the electrical charge of polymers [39, 52, 53]. Actually, polymer coating is widely used to reduce surface charge and suppress the EOF in CE [49, 54, 55].

Theoretical descriptions of the EOF of adsorbing polymers solutions are hardly found in the literature. It is worth noting that the existing models of electrokinetic phenomena in polymer-coated surfaces involve simple electrolyte solutions [56–59]. An interesting exception is [60], where the EOF was calculated by considering nonuniform (Newtonian) fluid viscosities near the capillary wall. A questionable aspect, however, is the definition of the plane of shear with the associated ζ -potential. It is known that determining the surface potential of polymer-covered surfaces poses several troubles, and the physical interpretation of measured values is sometimes ambiguous [39]. Charged polymers also undergo electrophoretic forces that compete with electroosmosis and make the problem much more complex (see for instance [45]). Actually, the characterization of interfaces with adsorbing charged polymers appears to challenge the standard electrokinetic model [61] and demands additional investigation.

In particular, if the attractive interaction energy between polymers and the surface is higher than thermal energy [3], the adhered chains form a compact, nondraining, solid-like layer. Silica surfaces for example are particularly susceptible to such a strong adsorption [62]. Under these conditions, the local viscosity strongly increases near the surface, and the shear rate virtually vanishes, meaning that the flow develops out of the adsorbed layer. As a first approximation, it is thought that the no-slip plane is shifted a distance δ_H into the channel, where δ_H is the so-called hydrodynamic thickness [63]. Electroosmosis can be certainly induced in these systems, provided an effective surface potential is present onto the adsorbed layer. Furthermore, given a compact coating, the EOF is defined by the chemistry of the adsorbed layer [64], and does not vary appreciably with the thickness δ_H [65]. Robust and stable coatings are achieved by using multiple ionic layers, and the procedure is normally used to control the EOF direction in CE [65, 66].

2.2 Polymer depletion and the apparent hydrodynamic slip

If the interaction between polymer molecules and the surface is nonattractive, the polymer segment concentration decreases steeply near the surface, and yields a polymer-depleted layer adjacent to the wall [2–6]. In fact, large molecules found less configurational entropy near solid boundaries, and hence they are naturally excluded from the interface. The effect is enhanced when channel walls and polymers chains have electrical charges of the same sign. In particular, if the polymer concentration completely vanishes, the fluid in the depletion layer is simply the solvent of the polymer solution. Under flow, relatively large shear rates develop in the interfacial region, as the local viscosity is lower than the bulk viscosity. From the macroscopic point of view, the effect is considered as an apparent slip at the wall, as shown schematically in Fig. 1.

The simplified picture described here could be certainly more complex in practice: hydrodynamic slip and dynamic

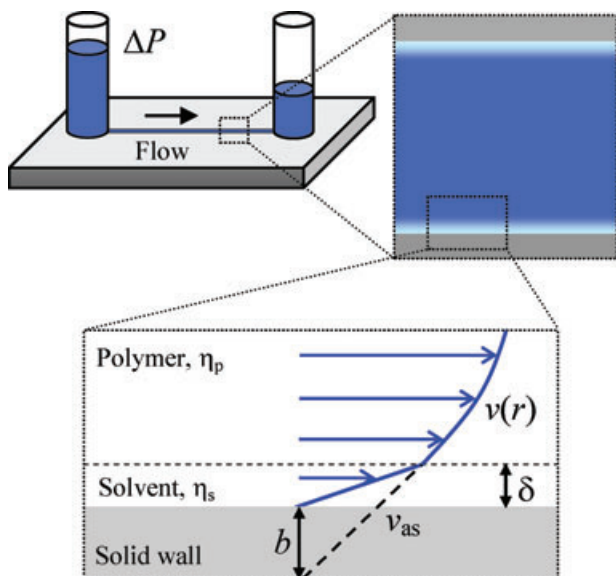


Figure 1. Schematic representations of an elementary microchannel connected to fluid reservoirs, filled with a solution of nonadsorbing polymers, and the corresponding fluid velocity profile, which presents an apparent hydrodynamic slip at the wall (not to scale).

adsorption/desorption could coexist under shear flow [1]; even if polymer molecules and surfaces have the same electrical charge, a certain degree of adsorption may occur due to specific interactions [29]; adsorption/depletion transitions may also occur in the presence of weakly charged chains or by adding salt [67]. Beyond these particular features, the apparent slip is normally observed in solutions of nonadsorbing polymers [10–14], as well as in a variety of colloidal systems (see [11] for a comprehensive review on the subject).

2.2.1 Pressure-driven flows

In flows driven by pressure gradients, the apparent slip yields flow rates higher than those predicted from the bulk viscosity, i.e. drag reduction is observed [11, 12]. Basically two approaches are used to describe these flows in the framework of continuum fluid mechanics: the two-fluid model, and the single-fluid model. In the first case, the flow on nonadsorbing polymers in cylindrical channels is modeled as the coaxial flow of two fluids: the central polymer solution and the cortical layer of solvent. Regarding the hydrodynamic resistance, the system is equivalent to a fluid with effective viscosity [68],

$$\eta_{\text{eff}} = \left[\frac{(1 - \delta/R)^4}{\eta_p} + \frac{1 - (1 - \delta/R)^4}{\eta_s} \right]^{-1}, \quad (1)$$

where the first term comes from the bulk polymer fluid with relatively high viscosity η_p , and the second is due to the layer of solvent adjacent to the wall with viscosity η_s (Fig. 1). Equation (1) indicates that the overall flow resistance of the polymer solution is lower than that of the bulk polymer (drag

reduction). Evidently, this model assumes a step-like function for the polymer concentration (hence the viscosity) in the interfacial region. More complete formulations introduce a linear decrease of polymer concentration in the depletion layer [69], and non-Newtonian behavior in the central zone [70].

On the other hand, the single fluid model considers uniform fluid properties in the flow domain, but replaces the no-slip boundary condition by an apparent slip velocity at the wall, as indicated by v_{as} in Fig. 1. This velocity is normally included in terms of the classic Navier condition, $v_{\text{as}} = -b(dv/dr)_{r=R}$, where b is the slip length, v is the fluid velocity, r is the radial coordinate, and R is the channel radius. Interestingly, it was shown [31] that this approach also yields Eq. (1) for $\delta \ll R$, provided the slip length is $b = \delta\eta_p/\eta_s$, as previously suggested for dilute polymer solutions [13, 14].

2.2.2 Electrophoresis

In electrophoresis of colloidal particles, experiments carried out by using solutions of nonadsorbing polymers as the background fluid usually lead to abnormally high electrophoretic mobilities. This result is quite reasonable if one takes into account that, for the ionic strength normally used, the thickness λ of the electrical double layer (EDL) is shorter than 10 nm. Therefore, as $\lambda < \delta$, the electrophoretic mobility of particles is determined by the viscosity of the depletion layer around them, which is lower than the bulk viscosity η_p . Actually, the first explanations given in terms of polymer depletion were reported two decades ago [27]. Mathematical models were improved later, where the two-fluid approach was used to include different viscosity profiles in the depletion layer: linear, exponential, and de Gennes' hyperbolic function [71, 72].

Given the paramount importance of the applications in this field, a better understanding of the phenomena involved is required. Recent theoretical calculations of electrophoretic mobility of particles in polymer solutions include the non-Newtonian character of the fluids, but assume uniform properties in the interfacial regions [73, 74]. Closely related to electrophoresis is the diffusive motion of particles through polymer solutions [15]; a recent study uses the two-fluid model to describe the relatively low hydrodynamic resistance due to polymer depletion around particle surfaces [75]. Additional complexity to this problem is given by the fact that the mixtures of colloidal particles and nonadsorbing polymers may undergo phase separation, precisely due to depletion interaction [76].

2.2.3 Electroosmosis

In electroosmosis, the effect of polymer depletion also manifests as an abnormally high mobility, or drag reduction, in relation to the EOF expected for the bulk properties of the

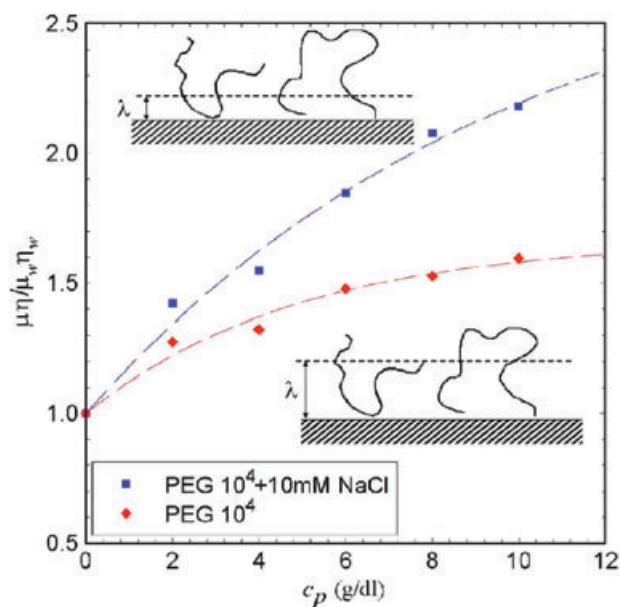


Figure 2. Drag reduction in the EOF of polymer solutions. Symbols are experimental data from PEG solutions in phosphate buffer (19.2 mM, pH 7). The lines are to guide the eyes. The insets schematically show the size of polymer chains in relation to EDL thickness. Reprinted with permission from [28]. Copyright 2007, American Institute of Physics.

polymer solution. Drag reduction was actually measured in EOF experiments carried out with solutions of poly-ethylene glycol in fused-silica capillaries [28]. Figure 2 shows the ratio $\mu_p \eta_p / \mu_s \eta_s$, where μ is the EOF mobility, as a function of polymer concentration c_p . It is clearly observed how drag reduction grows with c_p and, for a given c_p , drag reduction increases with ionic strength (smaller λ values). In fact, if the region where the EOF velocity develops is thinner than the average molecular size, polymer chains are only partially subjected to shear ($\lambda < \delta$; see the insets in Fig. 2). For the same reason, drag reduction also increases with polymer molecular weight, for a given λ [28]. In the limit of relatively large molecules, the EOF mobility is governed by η_s . This last result was also reported in [30], where poly-acrylamide solutions in glass microchannels were used.

The EOF mobility of aqueous solutions of carboxy-methyl cellulose in fused-silica capillaries was experimentally studied in [29]. Strong depletion was in principle expected at pH 7. Nevertheless, the formation of hydrogen bonds between macromolecules and silica surfaces leads to interfacial viscosities ranging between η_p and η_s . In addition, the non-Newtonian behavior of the polymer solution produced a nonlinear (electric field dependent) EOF mobility, as previously reported in [50]. When adsorption was inhibited by adding urea, the EOF mobility coincided to that of the BGE. Theoretical interpretations of these results were also given in [29].

The case of full polymer depletion has been described in [31], where the electrokinetic flow (electro-osmosis, streaming current, pressure-driven flow) of complex fluids in mi-

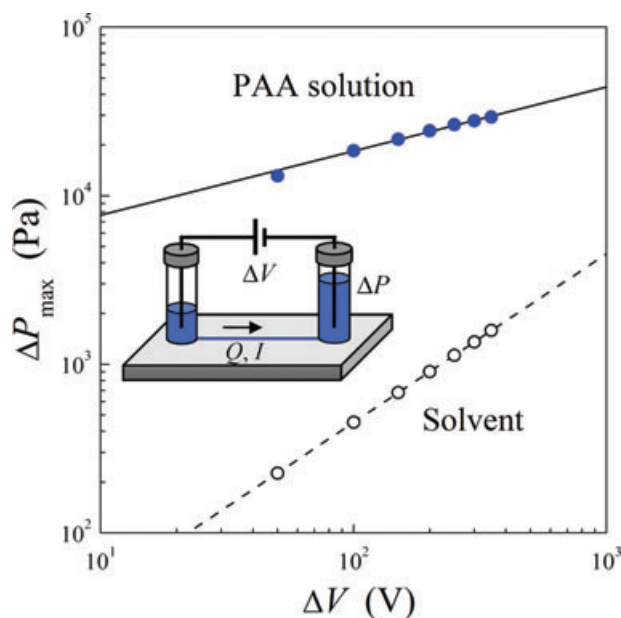


Figure 3. Enhancement of the maximum output pressure by using polymer solutions. Symbols are experimental data of polyacrylic acid (PAA) solutions (8.33 mM, 42 kD), and the respective solvent (10 mM Tris and 5 mM acetic acid in water, pH 8.2), from [89]. Lines are the prediction of the model proposed in [83]; see text for details.

crochannels was calculated by using the two-fluid approach. Expressions analogous to Eq. (1) for different non-Newtonian models (“power law”, Bingham, Eyring) were included, which are functions of the pressure gradient. The model successfully describes experimental data of EOF involving backpressure (see below Fig. 3, and the related text). Later calculations of the electrokinetic flow of non-Newtonian fluids also considered the presence of a depletion layer, and the two-fluid scheme [32, 33]. It is also relevant to mention a previous work dealing with numerical simulations of Carreau fluids in microchannels [77], where it was cleverly assumed that the EOF depends on the BGE only, considering that the EDL region is free of polymer molecules.

3 Implications

3.1 Electrokinetic flow

In a variety of microfluidic applications, the fluids are transported by applying pressure differences ΔP , and/or electric potential differences ΔV , which leads to coupled flows of matter and electricity. In steady and isothermal conditions, the flow rate Q and electric current I are described by [78, 79]:

$$Q = L_{11} \Delta P + L_{12} \Delta V, \quad (2)$$

$$I = L_{21} \Delta P + L_{22} \Delta V, \quad (3)$$

Table 1. Electrokinetic coefficients for cylindrical capillaries filled with Newtonian liquids of relatively thin EDL

Coefficients		L_{11}	L_{12}	L_{21}	L_{22}
Solvent ^{a)}		$-AR^2/(8\eta_s l)$	$A\varepsilon\zeta/(\eta_s l)$	$A\varepsilon\zeta/(\eta_s l)$	$-A\sigma/l$
Polymer solution	Wall depletion ^{b)}	$-AR^2/(8\eta_{\text{eff}} l)$	"	"	"
	Uniform properties ^{c)}	$-AR^2/(8\eta_p l)$	$A\varepsilon\zeta/(\eta_p l)$	$A\varepsilon\zeta/(\eta_p l)$	"

a) Simple electrolytes; A and l are the cross-sectional area and length of the channel, respectively, ε is the dielectric permittivity, and σ is the electrical conductivity of the fluid [81].

b) Fully deplete layers of thickness $\delta > \lambda$, where η_{eff} is given by Eq. (1); see [31] for expressions of non-Newtonian fluids.

c) Constant viscosity η_p in the region of the EDL; see [83] for expressions of non-Newtonian (power law) fluids.

where the coefficient L_{11} is the hydrodynamic conductance, $L_{12} = L_{21}$ are electroosmosis, and streaming phenomena, respectively (Onsager reciprocal relation), and L_{22} is the electric conductance. These linear force-flux relations allow one to model microfluidic networks by analogy with electrical circuits [80]. Table 1 presents the theoretical coefficients for simple electrolytes, Newtonian polymer solutions with wall depletion, and Newtonian polymer solutions with virtually uniform concentration in the interfacial region. These expressions involve the following considerations: (i) To satisfy the continuum hypothesis, calculations involve channels with radius R in the microscale, taking into account the size of discrete entities in solution (circa 10–100 nm for typical polymers). (ii) The thin EDL approximation applies ($R \gg \lambda$). (iii) Electrically neutral polymers are considered to avoid both electrophoretic forces that may compete with electroosmosis, and the formation of an additional EDL at the solvent-polymer solution interface.

In Table 1, the hydrodynamic conductance of nonadsorbing polymers includes η_{eff} , which is given by Eq. (1). Hence L_{11} depends on the bulk polymer viscosity, but it is a constant coefficient. If the polymer solution is non-Newtonian, which is generally the case, L_{11} is a function of ΔP [31]. Besides, for polymer-depleted layer of thickness $\delta > \lambda$, both electroosmosis and streaming current are governed by the local viscosity η_s , thus the electrokinetic coefficients coincide with those of the solvent, and Onsager reciprocity is satisfied. Further details on L_{12} and L_{21} for nonadsorbing polymers are given in [31]; here it is worth to add that these expressions assume that the channel ζ -potential is not altered by polymers chains, which in principle remain outside the EDL. Also in Table 1, the expression of the electric conductance L_{22} implicitly assumes that ionic mobilities are similar in both flow regions, which is valid for diluting polymer solutions, taking into account the variation of the conductivity σ with c_p [82].

Conductance coefficients for uniform polymer concentration were included in Table 1 for the purposes of comparison. These simple expressions are valid for Newtonian fluids only. In contrast, for non-Newtonian fluids, the EOF velocity is nonlinear with ΔV [29, 50], the streaming current is nonlinear with ΔP , and additional terms containing the product $\Delta V \Delta P$ arise in both Q and I [36, 83]. Precisely, a notable consequence of wall depletion is the decoupling of electrokinetic and non-Newtonian effects [31].

3.2 Electroosmotic pumping

EOP is a subject of intense research at present due to the extensive applications in microfluidics [84–88]. In these systems, electroosmosis works against a hydrodynamic load, as sketched in the inset of Fig. 3, thus the maximum output pressure (ΔP_{max} , reached when $Q = 0$; see Eq. (2) is a measure of the pump performance. It has been proven that ΔP_{max} can be substantially increased by using polymer solutions instead of simple electrolytes [89]. Figure 3 presents experimental data (symbols) obtained by using aqueous solution of poly-acrylic acid in silica capillaries. The demonstration that the effect is due to wall depletion, rather than to the non-Newtonian character of the fluid, was given later [83]. Precisely, the curves in Fig. 3 represent the theoretical modeling: the dashed line is the result for simple fluids, $\Delta P_{\text{max}}^{(s)} = -L_{12}^{(s)} \Delta V / L_{11}^{(s)}$, and the full line corresponds to a nonlinear relation $\Delta P_{\text{max}}^{(p)}(\Delta V)$ derived for power law fluids with wall depletion [83]; superscript (s) and (p) stand for solvent and polymer, respectively. In what follows, the concept is revisited by using the simple picture of Newtonian fluids described above, in order to highlight the effect of wall depletion.

The relationship between Q and ΔP given by Eq. (2), the so-called pump curve, is plotted in Fig. 4 for typical parameter values. It is observed that the maximum flow rate (at $\Delta P = 0$) attained with the polymer solution coincides with that of the solvent, because electroosmosis is determined by the viscosity of the depletion layer. However, the maximum output pressure is notably higher than that of the solvent. The corresponding velocity profiles for a given pressure load are plotted in the inset of Fig. 4. First, it is worth to remember that if $\Delta P = 0$ the fluid velocity is uniform throughout the cross-sectional area of the channel, and velocity gradients are limited to a thin region adjacent to the interface. When a counterpressure is present, the net flow results from the combination of the forward EOF and the backward pressure-driven flow. The velocity profiles in Fig. 4 correspond to ΔP around 70 Pa. This pressure load yield $Q = 0$ for the pure solvent (the backflow compensates electroosmosis), but it is not sufficient to generate a backflow in the polymer solution, due to the high hydrodynamic resistance of the bulk polymer. The electroosmotic forces acting in the interfacial layer drag the polymeric fluid as a plug, with a slightly indented velocity profile. Thus the polymeric liquid provides a relatively high output pressure.

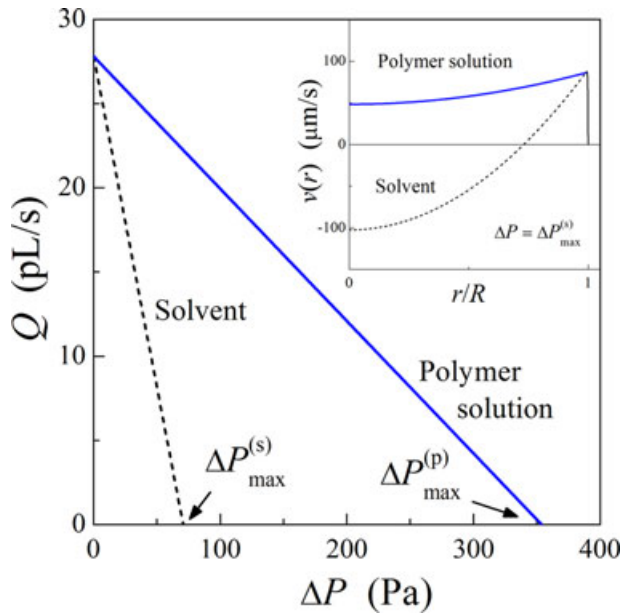


Figure 4. Flow rate as a function of the backpressure for the EOP of a polymer solution, compared to the solvent under the same experimental conditions. The inset shows the respective velocity profiles, at the backpressure value that makes $Q = 0$ for the solvent. Parameter values used in calculations are $\eta_s = 1$ mPas; $\eta_p = 5\eta_s$; $l = 1$ cm; $R = 10$ μ m; $\delta = 100$ nm; $\varepsilon = 7.1 \times 10^{-10}$ C²/Nm²; $\zeta = -25$ mV; $\Delta V = 50$ V.

In terms of the conductance coefficients, the bulk polymer yields a diminution of L_{11} without affecting L_{12} , which only depends on η_s . Therefore, the maximum pressure attained with the polymer solution in relation to the solvent without polymer is:

$$\frac{\Delta P_{\max}^{(p)}}{\Delta P_{\max}^{(s)}} = \frac{L_{11}^{(s)}}{L_{11}^{(p)}}. \quad (4)$$

By using the expressions reported in Table 1, the above ratio results,

$$\frac{L_{11}^{(s)}}{L_{11}^{(p)}} = \frac{1}{1 + (\eta_s/\eta_p - 1)(1 - \delta/R)^4}. \quad (5)$$

The prediction of this equation is shown in Fig. 5. In the limit $\delta/R \ll 1$, $L_{11}^{(s)}/L_{11}^{(p)} \approx \eta_p/\eta_s$, which clearly shows the gain of output pressure in relation to simple electrolytes. In the limit $\eta_p/\eta_s \gg 1$, the ratio δ/R becomes the controlling factor. In any case, $L_{11}^{(s)}/L_{11}^{(p)} > 1$, given that η_p is always higher than η_s .

The above results are relevant because they also mean an improvement of the thermodynamic efficiency, which is the main concern in EOP [90–94]. The efficiency is defined as the ratio of the useful mechanical power to the electrical power consumption $\chi = \Delta P Q / (-\Delta V I)$ [95]. By using Eqs. (2) and (3), the efficiency can be expressed,

$$\chi = \frac{1 - \Delta P/\Delta P_{\max}}{L_{22}\Delta V/(L_{21}\Delta P) - 1}. \quad (6)$$

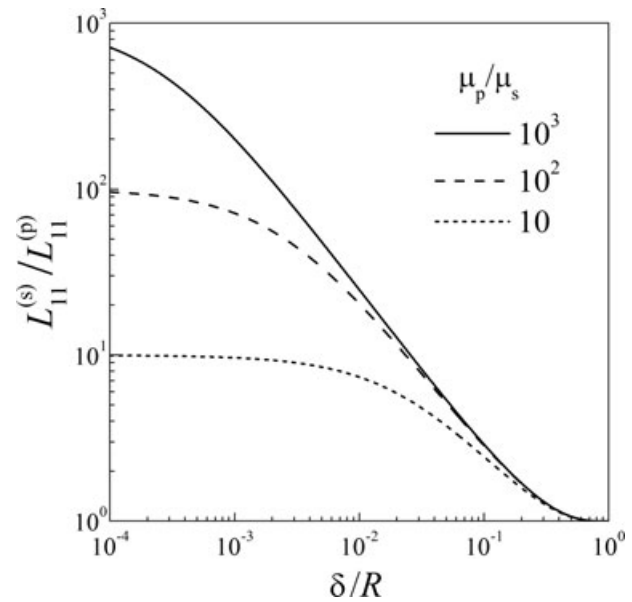


Figure 5. Ratio of the conductance coefficients for solvent and polymer solution, as a function of relative depletion layer thickness, according to Eq. (5). The ratio represents both the relative output pressure, Eq. (4), and the relative efficiency, Eq. (9), of electrokinetic energy converters.

The maximum efficiency χ_{\max} is obtained by maximizing Eq. (6) in relation to the applied pressure ($\partial\chi/\partial\Delta P = 0$), for a given ΔV and constant conductance coefficients. If one further considers that $L_{21}\Delta P \ll L_{22}\Delta V$, which is valid for typical parameter values, it is readily found that χ_{\max} is reached at $\Delta P = \Delta P_{\max}/2$ [84, 85], and may be written simply [93],

$$\chi_{\max} = \frac{1}{4} \frac{L_{12}^2}{L_{11}L_{22}}. \quad (7)$$

In the case of solutions of nonadsorbing polymers, provided they are Newtonian, conductance coefficients are constant (ΔP independent), thus the maximization described above also leads to,

$$\chi_{\max}^{(p)} = \frac{1}{4} \frac{L_{12}^{(p)^2}}{L_{11}^{(p)}L_{22}^{(p)}}. \quad (8)$$

By ratiocinating the above expressions, and taking into account that electrokinetic coefficients are equal to those of the solvent (Table 1), the maximum efficiency of the polymer solution in relation to the solvent results,

$$\frac{\chi_{\max}^{(p)}}{\chi_{\max}^{(s)}} = \frac{L_{11}^{(s)}}{L_{11}^{(p)}}. \quad (9)$$

This ratio coincides with the prediction of Eq. (4), which is plotted in Fig. 5. Therefore, a notable increase of the EOP efficiency is predicted when nonadsorbing polymer solutions are employed as the working fluid.

3.3 Power generation

Energy harvesting from small flows is a hot topic at present, motivated by the search for alternative energy sources in microdevices [96]. In particular, power generation by means of streaming current has experienced a renaissance with the advent of micro and nanofluidics [97–103], and constant efforts are being made to improve the conversion efficiency [104–108]. In the framework of Eq. (3), pressure-driven flows induce the streaming current due to the convective transport of excess ions in solution. A streaming potential is also induced in the opposite direction, thus the net electric current that can be supplied to an external load results from the difference between the forward and backward fluxes of charge.

The efficiency of the process is defined as the ratio of the useful electrical power to the mechanical power consumption $\chi = \Delta V I / (-\Delta P Q)$ [95]. By using Eqs. (2) and (3), the efficiency results,

$$\chi = \frac{1 - \Delta V / \Delta V_{\max}}{L_{11} \Delta P / (L_{12} \Delta V) + 1}, \quad (10)$$

where $\Delta V_{\max} = -L_{21} \Delta P / L_{22}$. By maximizing the efficiency in relation to the applied voltage ($\partial \chi / \partial \Delta V = 0$), for a given ΔP and constant conductance coefficients, and taking into account that $L_{12} \Delta V \ll L_{11} \Delta P$ (see also [98]), it is found that the maximum is reached at $\Delta V = \Delta V_{\max} / 2$, and that χ_{\max} coincides to Eq. (7) ([93]).

In the case of Newtonian solutions of nonadsorbing polymers, the hydrodynamic conductance is a constant (it does not depend on ΔV), and electrokinetic coefficients are equal to those of the solvent (Table 1). Thus the maximization of the power generation also leads to Eq. (8). Consequently, the prediction of Eq. (9) applies for power generation as well, and a remarkable increase of the streaming current efficiency is expected with nonadsorbing polymers [109]. More recent calculations [110] reinforce these arguments.

It should be noted that, in contrast to the case of EOP, the generated power is not increased by the polymer solution. The gain of the efficiency is entirely given by the diminution of the mechanical power consumption. Again this is a consequence of wall depletion, and can be rationalized as follows. For relatively small λ , the current density due to streaming is confined to a thin layer adjacent to the interface, and results $j = -\varepsilon \zeta |dv/dr|_{r=R}$ [111]. The wall shear rate is determined by the fluid onto the wall, and hence it is equal for both pure solvent and wall-depleted polymer solution, for a given ΔP , as illustrated in Fig. 6. Therefore, under the same experimental conditions, both systems yield the same generated power. Nevertheless, the presence of the polymer increases the overall hydrodynamic resistance, leading to a relatively lower Q for a given ΔP .

From a practical point of view, $\chi_{\max}^{(p)} / \chi_{\max}^{(s)}$ around 10^3 could be reached with proper formulations of the working fluid. Considering that $\chi_{\max}^{(s)} \sim 10^{-5}$ for simple electrolytes in microchannels, absolute efficiencies $\chi_{\max}^{(p)} \sim 1\%$ are in principle achievable with polymer solutions. This value is still lower than the best performances obtained with nanoscale

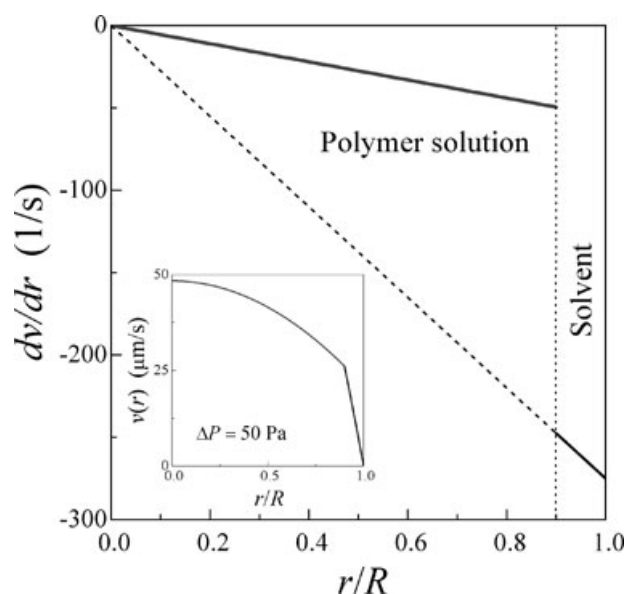


Figure 6. Shear rate profile for the pressure-driven flow of Newtonian polymer solutions with wall depletion. The inset shows the corresponding fluid velocity. The dotted line indicates the shear rate of the pure solvent. Parameter values used in calculations are $\eta_s = 1$ mPas; $\eta_p = 5\eta_s$; $l = 1$ cm; $R = 10$ μm ; $\delta = 1$ μm ; $\Delta P = 50$ Pa.

channels and extremely low ionic strengths (see, for instance [99, 101]). One should note, however, that polymer solutions involve microscale channels and moderate ionic strengths.

Finally, it is worth to point out that the predicted χ_{\max} is equal for generation and pumping modes only if the polymer solution has a Newtonian viscosity. In the more general case of non-Newtonian fluids, the efficiency of power generation is a function of ΔP [109], and differs from the corresponding result for EOP, which is a function of ΔV [83].

4 Concluding remarks

Throughout this work, the evidences of wall depletion and apparent slip were re-examined, and relevant consequences of these phenomena on the dynamics of electrokinetic flow were discussed. The topic is of fundamental interest, and has many practical motivations.

The first remark to be made is that complex fluids involve a series of physical effects at solid–liquid interfaces, beyond its non-Newtonian behavior. A key feature is the presence of discrete entities with sizes in the range of nano to micrometers. The distribution of these entities is unavoidably distorted in the vicinity of channel walls and, consequently, physical properties like viscosity are nonuniform in the EDL region. Therefore, any approach to describe electrokinetic phenomena of non-Newtonian fluids necessarily has to consider these interfacial effects.

A second remark is the possibility to capitalize the apparent slip phenomenon in practical applications such as microfluidic pumping and energy harvesting that are research

fields of intense activity at present. The evidences that nonadsorbing polymer solutions reduce the EOF drag and substantially increase the EOP efficiency are proofs of the concept. In a broader sense, a better understanding of wall depletion and slip phenomena would allow one to engineer both fluids and surfaces with enhanced properties for defined purposes in electrokinetics.

The author acknowledges the financial support from CONICET (PIP 0317), and Universidad Nacional del Litoral (CAI+D 65/328), Argentina.

The author has declared no conflict of interest.

5 References

- [1] Nghe, P., Terriac, E., Schneider, M., Li, Z. Z., Cloitre, M., Abecassis, B., Tabeling, P., *Lab Chip* 2011, 11, 788–797.
- [2] de Gennes, P.-G., *Adv. Colloid Interf. Sci.* 1987, 27, 189–209.
- [3] Israelachvili, J., *Intermolecular and Surface Forces*, Academic Press, London 1997.
- [4] Netz, R. R., Andelman, D., *Phys. Rep.* 2003, 380, 1–95.
- [5] Flier, G. J., *Adv. Colloid Interf. Sci.* 2010, 159, 99–116.
- [6] Wang, Y., Hansen, F. Y., Peters, G. H., Hassager, G. H., *J. Chem. Phys.* 2008, 129, 074904.
- [7] Agarwal, U. S., Dutta, A., Mashelkar, R. A., *Chem. Eng. Sci.* 1994, 49, 1693–1717.
- [8] Ma, H., Graham, M. D., *Phys. Fluid* 2005, 17, 083103.
- [9] Taniguchi, T., Arai, Y., Tuinier, R., Fan, T. H., *Eur. Phys. J. E* 2012, 35, 88.
- [10] Schowalter, W. R., *J. Non-Newtonian Fluid Mech.* 1988, 29, 25–36.
- [11] Barnes, H. A., *J. Non-Newtonian Fluid Mech.* 1995, 56, 221–251.
- [12] Granick, S., Zhu, Y., Lee, H., *Nat. Mater.* 2003, 2, 221–227.
- [13] Tuinier, R., Taniguchi, T., *J. Phys. Condens. Matter* 2005, 17, L9–L14.
- [14] Degré, G., Joseph, P., Tabeling, P., Lerouge, S., Cloitre, M., Adjari, A., *Appl. Phys. Lett.* 2006, 89, 024104.
- [15] Hoogendam, C. W., Peters, J. C. W., Tuinier, R., de Keizer, A., Cohen Stuart, M. A., Bijsterbosch, B. H., *J. Colloid Interf. Sci.* 1998, 207, 309–316.
- [16] Neto, C., Evans, D. R., Bonaccorso, E., Butt, H.-J., Craig, V. S. J., *Rep. Prog. Phys.* 2005, 68, 2859–2897.
- [17] Lauga, E., Brenner, M. P., Stone, H. A., in: Tropea, C., Yarin, A., Foss, J. (Eds.), *Handbook of Experimental Fluid Dynamics*, Springer, New-York 2007, pp. 1219–1240.
- [18] Eijkel, J., *Lab Chip* 2007, 7, 299–301.
- [19] de Gennes, P. G., *Langmuir* 2002, 18, 3413–3414.
- [20] Gad-el-Hak, M., *Phys. Fluids* 2005, 17, 100612.
- [21] Harting, J., Kunert, C., Hyvälouma, J., *Microfluid. Nanofluid.* 2010, 8, 1–10.
- [22] Ajdari, A., Bocquet, L., *Phys. Rev. Lett.* 2006, 96, 186102.
- [23] Bouzigues, C. I., Tabeling, P., Bocquet, L., *Phys. Rev. Lett.* 2008, 101, 114503.
- [24] Squires, T. M., *Phys. Fluids* 2008, 20, 092105.
- [25] Tandon, V., Kirby, B. J., *Electrophoresis* 2008, 29, 1102–1114.
- [26] Park, H. M., *Electrophoresis* 2012, 33, 906–915.
- [27] Donath, E., Kuzmin, P., Krabi, A., Voigt, A., *Colloid Polym. Sci.* 1993, 271, 930–939.
- [28] Chang, F. M., Tsao, H. W., *Appl. Phys. Lett.* 2007, 90, 194105.
- [29] Olivares, M. L., Vera-Candiotti, L., Berli, C. L. A., *Electrophoresis* 2009, 30, 921–929.
- [30] Bryce, R. M., Freeman, M. R., *Phys. Rev. E* 2010, 81, 036328.
- [31] Berli, C. L. A., Olivares, M. L., *J. Colloid Interf. Sci.* 2008, 320, 582–589.
- [32] Liu, Q., Jian, Y., Yang, L., *Phys. Fluids* 2011, 23, 102001.
- [33] Sousa, J. J., Afonso, A. M., Pinho, F. T., Alves, M. A., *Microfluid. Nanofluid.* 2011, 10, 107–122.
- [34] Chakraborty, S., *Anal. Chim. Acta* 2007, 605, 175–184.
- [35] Park, H. M., Lee, W. M., *J. Colloid Interf. Sci.* 2008, 317, 631–636.
- [36] Afonso, A. M., Alves, M. A., and Pinho, F. T., *J. Non-Newtonian Fluid Mech.* 2009, 159, 50–63.
- [37] Tang, G. H., Ye, P. X., Tao, W. Q., *J. Non-Newtonian Fluid Mech.* 2010, 165, 435–440.
- [38] Cho, C.-C., Chen, C.-L., Chen, C.-K., *Electrophoresis* 2012, 33, 743–750.
- [39] Delgado, A. V., González-Caballero, F., Hunter, R. J., Koopal, L. K., Lyklema, J., *J. Colloid Interf. Sci.* 2007, 309, 194–224.
- [40] Viovy, J. L., *Rev. Mod. Phys.* 2000, 72, 813–872.
- [41] Slater, G. W., Guillouze, S., Gauthier, M. G., Mercier, J. F., Kenward, M., McCormic, L. C., Tessier, F., *Electrophoresis* 2002, 23, 3791–3816.
- [42] Buchholz, B. A., Shi, W., Barron, A. E., *Electrophoresis* 2002, 23, 1398–1409.
- [43] van Heiningen, J. A., Mohammadi, A., Hill, R. J., *Lab Chip* 2010, 10, 1907–1921.
- [44] Mohammadi, A., Hill, R. J., *J. Fluid Mech.* 2011, 669, 298–327.
- [45] Mohammadi, A., van Heiningen, J. A., Hill, R. J., *Soft Matter* 2012, 8, 8094–8106.
- [46] Bird, R. B., Armstrong, R., Hassager, O., *Dynamics of Polymeric Liquids*, Vol. 1, J. Wiley & Sons, New York 1977.
- [47] Semenov, A. N., Bonet-Avalos, J., Johnner, A., Joanny, J. F., *Macromolecules* 1996, 29, 2179–2196.
- [48] Dobrynin, A. V., Obukhov, S. P., Rubinstein, M., *Macromolecules* 1999, 32, 5689–5700.
- [49] Hjertén, S., *J. Chromatogr.* 1985, 347, 191–198.
- [50] Bello, M. S., de Besi, P., Rezzonico, R., Righetti, P. G., Casiraghi, E., *Electrophoresis* 1994, 15, 623–626.
- [51] Mazzeo, J. R., Krull, I. S., *Anal. Chem.* 1991, 63, 2852–2857.

- [52] Righetti, P. G., Gelfi, C., Verzola, B., Castelletti, L., *Electrophoresis* 2001, 22, 603–611.
- [53] Danger, G., Ramonda, M., Cottet, H., *Electrophoresis* 2007, 28, 925–931.
- [54] Cretich, M., Chiari, M., Pirri, G., Crippa, A., *Electrophoresis* 2005, 265, 1913–1919.
- [55] Kaneta, T., Ueda, T., Hata, K., Imasaka, T., *J. Chromatogr. A* 2006, 1106, 52–55.
- [56] Ohshima, H., *Adv. Colloid Interf. Sci.* 1995, 62, 189–235.
- [57] Cohen, J. A., Khorosheva, V. A., *Colloid. Surface. A* 2001, 195, 113–127.
- [58] Duval, J. F. L., *Langmuir* 2005, 21, 3247–3258.
- [59] Langlet, J., Gaboriaud, F., Gantzer, C. Duval, J. F. L., *Biophys. J.* 2008, 94, 3293–3312.
- [60] Otevřel, M., Klepárník, K., *Electrophoresis* 2002, 23, 3574–3582.
- [61] Dukhin, S. S., Zimmermann, R., Werner, C., *J. Colloid Interf. Sci.* 2008, 328, 217–226.
- [62] Parida, S. K., Dash, S., Patel, S., Mishra, B. K., *Adv. Colloid Interf. Sci.* 2006, 121, 77–110.
- [63] Cohen Stuart, M. A., Waajen, F. H. W. H., Cosgrove, T., Vincent, B., Crowley, T. L., *Macromolecules* 1984, 17, 1825–1830.
- [64] Burns, N. L., Van Alstine, J. M., Harris, J. M., *Langmuir* 1995, 11, 2768–2776.
- [65] Boonsong, K., Caulum, M. M., Dressen, B. M., Chailapakul, O., Crokek, D. M., Henry, C. S., *Electrophoresis* 2008, 29, 3128–3134.
- [66] Graul, T. W., Schlenoff, J. B., *Anal. Chem.* 1999, 71, 4007–4013.
- [67] Shafir, A., Andelman, D., Netz, R. R., *J. Chem. Phys.* 2003, 119, 2355–2362.
- [68] Chauveteau, G., *J. Rheol.* 1982, 26, 111–142.
- [69] Sorbie, K. S., *J. Colloid Interf. Sci.* 1990, 139, 299–314.
- [70] Lopez X., Valvatne, P. H., Blunt, M., *J. Colloid Interf. Sci.* 2003, 264, 256–265.
- [71] Donath, E., Krabi, A., Allan, G., Vincent, B., *Langmuir* 1996, 12, 3425–3430.
- [72] Zhivkov, A. M., *J. Colloid Interf. Sci.* 2007, 313, 122–127.
- [73] Lee, E., Huang, Y. F., Hsu, J. P., *J. Colloid Interf. Sci.* 2003, 258, 283–288.
- [74] Khair, A. S., Posluszny, D. E., Walker, L. M., *Phys. Rev. E* 2012, 85, 016320.
- [75] Fan, T.-H., Dhont, J. K. G., Tuinier, R., *Phys. Rev. E* 2007, 75, 011803.
- [76] Anderson, V. J., Lekkerkerker, H. N. W., *Nature* 2002, 416, 811–815.
- [77] Zimmerman, W. B., Rees, J. M., Craven, T. J., *Microfluid. Nanofluid.* 2006, 2, 481–492.
- [78] de Groot, S. R., *Thermodynamics of Irreversible Processes*, North-Holland Publishing, Amsterdam 1951.
- [79] Brunet, E., Adjari, A., *Phys. Rev. E* 2004, 69, 016306.
- [80] Berli, C. L. A., *Microfluid. Nanofluid.* 2008, 4, 391–399.
- [81] Rice, C. L., Whitehead, R., *J. Phys. Chem.* 1965, 69, 4017–4024.
- [82] Wang, S. C., Tsao, H. K., *Macromolecules* 2003, 36, 9128–9134.
- [83] Berli, C. L. A., *Microfluid. Nanofluid.* 2010, 8, 197–207.
- [84] Laser, D. J., Santiago, J. G., *J. Micromech. Microeng.* 2004, 14, R35–R64.
- [85] Wang, P., Chen, Z., Chang, H.-C., *Sens. Act. B* 2006, 113, 500–509.
- [86] Edwards, IV, J. M., Hamblin, M. N., Fuentes, H. V., Peeni, B. A., Lee, M. L., Woolley, A. T., Hawkins, A. R., *Biomicrofluidics* 2007, 1, 014101.
- [87] Iverson, B. D., Garimella, S. V., *Microfluid. Nanofluid.* 2008, 5, 145–174.
- [88] Wang, X., Cheng, C., Wang, S., Liu, S., *Microfluid. Nanofluid.* 2009, 6, 145–162.
- [89] Phillip, H. P., Patent WO 2006/068959 A2, 2006.
- [90] Chen, C.-H., Santiago, J. G., *J. Microelectromech. Syst.* 2002, 11, 672–683.
- [91] Min, J. Y., Hasselbrink, E. F., Kim, S. J., *Sens. Act. B* 2004, 98, 368–377.
- [92] Griffiths, S. K., Nilson, R. H., *Electrophoresis* 2005, 26, 351–361.
- [93] Xuan, X., Li, D., *J. Power Sources* 2006, 156, 677–684.
- [94] Chein, R., Liao, J., *Electrophoresis* 2007, 28, 635–643.
- [95] Morrison Jr., F. A., Oesterle, J. F., *J. Chem. Phys.* 1965, 43, 2111–2115.
- [96] Pennathur, S., Eijkel, J., van den Berg, A., *Lab Chip* 2007, 7, 1234–1237.
- [97] Yang, J., Lu, F., Kostiuik, L. W., Kwok, D. Y., *J. Micromech. Microeng.* 2003, 13, 963–970.
- [98] Olthuis, W., Schippers, B., Eijkel, J., van den Berg, A., *Sens. Act. B* 2005, 111–112, 385–389.
- [99] van der Heyden, F. H. J., Bonthuis, D. J., Stein, D., Meyer, C., Dekker, C., *Nano Lett.* 2007, 7, 1022–1025.
- [100] Duffin, A. M., Saykally, R. J., *J. Phys. Chem. C* 2008, 112, 17018–17022.
- [101] Xie, Y., Wang, X., Xue, J., Jin, K., Chen, L., Wang, Y., *Appl. Phys. Lett.* 2008, 93, 163116.
- [102] Choi, Y. S., Kim, S. J., *J. Colloid Interf. Sci.* 2009, 333, 672–678.
- [103] Dhiman, P., Yavari, F., Mi, X., Gullapalli, H., Shi, Y., Ajayan, P. M., Koratkar, N., *Nano Lett.* 2011, 11, 3123–3127.
- [104] van der Heyden, F. H. J., Bonthuis, D. J., Stein, D., Meyer, C., Dekker, C., *Nano Lett.* 2006, 6, 2232–2237.
- [105] Ren, Y., Stein, D., *Nanotechnology* 2008, 19, 195707.
- [106] Davidson, C., Xuan, X., *Electrophoresis* 2008, 29, 1125–1130.
- [107] Xie, Y., Sherwood, J. D., Shui, L., van den Berg, A., Eijkel, J., *Lab Chip* 2011, 11, 4006–4011.
- [108] Gillespie, D., *Nano Lett.* 2012, 12, 1410–1416.
- [109] Berli, C. L. A., *J. Colloid Interf. Sci.* 2010, 349, 446–448.
- [110] Bandopadhyay, A., Chakraborty, S., *Langmuir* 2011, 27, 12243–12252.
- [111] Brunet, E., Adjari, A., *Phys. Rev. E* 2006, 73, 056306.